W/Z boson properties, including W mass, at the Tevatron

Jan Stark
(for the CDF and DØ Collaborations)
Laboratoire de Physique Subatomique et de Cosmologie, IN2P3-CNRS, Université Grenoble 1, Institut National Polytechnique de Grenoble, Grenoble, France

The mass of the W boson, m_W, is a free parameter in the standard model. Measurements of this parameter are a key ingredient to indirect limits on the mass of the hypothetical Higgs boson. The uncertainty in the predicted Higgs mass is currently driven by the experimental uncertainty in m_W. We present a new preliminary measurement of the W boson mass by DØ based on 1 fb^{-1} of data from Run II of the Fermilab Tevatron. This measurement is presented for the first time at this conference, and it is the single most precise measurement to date. We compare this measurement to the earlier Run II measurement published by CDF, and we review the excellent prospects for further improvement in both of these measurements as well as in their combination. We briefly discuss a new W boson charge asymmetry by CDF. It will further constrain the parton density functions (PDFs). PDFs are inputs to many measurements performed at hadron colliders, including the measurement of m_W.

1 Introduction

As is well known, predicting the values of particle masses is not one of the strengths of the standard model (SM). The mass of the W boson, m_W, is not an exception, but the SM does predict a relation between m_W and other experimental observables:

$$m_W = \sqrt{\frac{\pi\alpha}{\sqrt{2}G_F}} \frac{1}{\sin\theta_W \sqrt{1-\Delta r}} ,$$

where α is the fine structure constant, G_F is the Fermi constant and θ_W denotes the Weinberg angle. The radiative corrections Δr are of the order of 4%. In the SM, Δr receives sizeable contributions from the one-loop diagram with top and bottom quarks that is shown in Fig. 1, as well as Higgs one-loop contributions from diagrams like *e.g.* the one shown in Fig. 1. As a consequence, Δr depends on m_t, the mass of the top quark, as $\sim m_t^2$ and on m_H, the mass

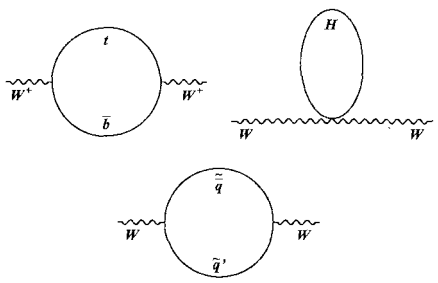

Figure 1: One-loop contributions to the W boson mass from top and bottom quarks (top left) and an example of the Higgs one-loop corrections (top right). The diagram at the bottom is an example of one-loop squark contributions in supersymmetric extensions to the SM. Reproduced from Ref. [1].

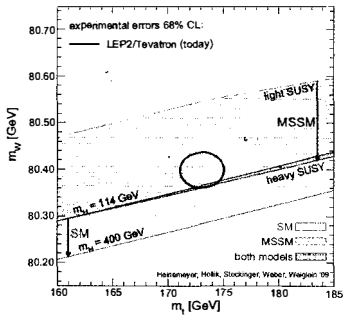

Figure 2: Current world averages for top quark and W boson masses, compared to SM predictions for different Higgs boson masses ($m_H = 114$ GeV corresponds to the present lower limit from direct Higgs searches), as well as to a SUSY extension of the SM. Taken/updated from [2].

of the hypothetical Higgs boson, as $\sim \log m_H$. Given the above relation, precise measurements of both the top quark mass and the W boson mass[a] can be translated into a prediction of the mass of the hypothetical Higgs boson. This is an important piece of information that can be used as guidance for where to look for the Higgs boson, maybe even to rule out the SM Higgs boson if the prediction should become inconsistent with limits from direct searches, or to test the consistency of the SM if the Higgs is found and its mass measured directly. The experimental uncertainties in the top quark mass, Δm_t, and in the W boson mass, Δm_W, contribute equality to the uncertainty in the predicted Higgs mass if $\Delta m_W \simeq 0.006 \times \Delta m_t$. The current Tevatron average of the top quark mass is $m_t = 173.1 \pm 1.3$ GeV. In order to match this precision, one would need $\Delta m_W = 8$ MeV, which is far away from the precision of the current world average, $\Delta m_W = 25$ MeV. The experimental uncertainty in the W boson mass is and will be the limiting factor for many years to come and needs to be reduced. Additional contributions to Δr arise in various extensions to the SM, *e.g.* in supersymmetry via diagrams like the one shown at the bottom of Fig. 1. The current situation is summarised in Fig. 2.

2 A new measurement of the W boson mass from DØ

W bosons are copiously produced at the Tevatron $p\bar{p}$ collider. In this environment, mass measurements use $W \to e\nu$ and $W \to \mu\nu$ decays to clean leptonic final states. The W boson mass is typically extracted from three experimental observables, namely the distributions of the lepton transverse momentum p_T^ℓ, the transverse momentum of the neutrino p_T^ν, as inferred from the missing transverse energy $\not\!\!E_T$, $p_T^\nu = \not\!\!E_T$, and the *transverse mass* $m_T = \sqrt{2p_T^\ell p_T^\nu(1-\cos\Delta\phi)}$, where $\Delta\phi$ is the angle in the transverse plane between the lepton and the neutrino. The principle is simple: *e.g.* a larger value of m_W would lead to larger average p_T^ℓ. In practice, we use a Monte Carlo simulation that predicts the shape of our three observables for a given input mass hypothesis. The mass hypothesis is then adjusted to obtain the best description of the data. The Monte Carlo simulation includes two parts: a "physics" generator that models the W boson production and decay kinematics, followed by a parameterised model of the detector response to the lepton and the *hadronic recoil* $\vec{u}_T$, *i.e.* all other particles that recoil against the W boson, $-\vec{\not\!\!E}_T = \vec{p}_T^{\,\ell} + \vec{u}_T$. In order to achieve the level of uncertainties that has been discussed above, one needs to understand the lepton energy scale at the 0.2 per-mil level and the hadronic recoil

[a] Plus all the other observables in the equation; and they are very well measured.

energy scale at the 1% level. These requirements, especially on the lepton energy scale, are extremely stringent and require a precise understanding of the detectors. A much more detailed discussion of the techniques of m_W measurements at the Tevatron can be found in Ref. [3].

The DØ Collaboration has completed its first preliminary measurement of m_W in Run II, and it is presented in public for the first time at this conference. A more detailed description of the measurement can be found in Ref. [4]. The "physics" part of the simulation is based on the ResBos generator [5] using the CTEQ6.1M PDF set [6], and interfaced with Photos [7] to model final state radiation (FSR).
This measurement uses only the channel $W \to e\nu$ with central electrons (detector $|\eta| \ o \ 1.05$). The radius of DØ's magnetic central tracking system is very small, leading to a poor momentum resolution. Consequently, a measurement of m_W in the muon channel is much less competitive and more difficult than in the electron channel [3]. Electron energies are measured using the DØ liquid argon calorimeter, and central tracking does provide precise direction measurements for electrons. The DØ calorimeter has reasonably good energy resolution, it has very good linearity and it is very stable over time (thanks to the "unit gain" nature of the readout). It is rather hermetic, which gives us relatively precise measurements of the hadronic recoil, and its readout is finely segmented, including in the direction longitudinal to the shower development.
Central electrons are required to pass $p_T^e > 25$ GeV and strict identification criteria. W candidate events are required to have one electron candidate, $\not\!\!E_T > 25$ GeV and $u_T \ o \ 15$ GeV. $Z \to ee$ candidate events are required to have two electron candidates and $u_T \ o \ 15$ GeV. In 1 fb^{-1} of data these requirements yield 18,725 Z candidates with negligible background, and 499,830 W candidates with a signal purity of 96% (residual backgrounds arise from $W \to \tau\nu \to e\nu\nu$ events, QCD multijet events in which one jet is misidentified as an electron and $\not\!\!E_T$ arises from misreconstruction. and $Z \to ee$ events in which one electron escaped into a poorly instrumented region of the detector). The Z peak is shown in Fig. 3; this sample is the key control sample in the DØ analysis that makes it possible to tune the parameterised detector simulation at a great level of detail and to achieve the precision discussed above. For example, we use this sample, as well as the precise measurement of m_Z from LEP to set the absolute electron energy scale. This sample is further used to measure the constant term in the calorimeter resolution (using the width of the measured Z peak), to measure electron identification and trigger efficiencies (because a clean sample of Z events can be selected using tight requirements on just one of the two electrons, leaving the other one relatively unbiased), and to calibrate the recoil energy measurements. The comparatively small size of the Z sample is therefore a limiting factor.
DØ use relatively inclusive samples of EM-like events to uniformise the calorimeter response in ϕ, and $Z \to ee$ events to set the absolute energy scale in bins of detector η. But electrons from $Z \to ee$ have an energy/rapidity-spectrum that is slightly different from the spectrum of electrons from $W \to e\nu$: at a given rapidity, electrons from W decay have an energy spectrum that is lower on average. Intrinsically, the DØ LAr calorimeter has good linearity, and energy offsets from recoil energy flowing into the electron window are modelled explicitly in the fast detector simulation. The main non-linearities arise from energy losses in the uninstrumented material in front of the calorimeter. These are corrected for using a detailed first-principles simulation. One key ingredient to this simulation is a map of all material inside and in front of the calorimeter from a first-principles accounting (*i.e.* based on known detector geometry and material properties). The cumulative amount of uninstrumented material is particularly critical. We use electrons from $Z \to ee$ and the longitudinal segmentation of the DØ calorimeter to check the total mount of uninstrumented material in bins of rapidity. Figure 4 illustrates how the average electron shower is sampled in DØ Run II. From the figure it is clear that the fractional electron energy depositions in each of the four EM readout sections are very sensitive to the amount of uninstrumented material. After a 5% correction (uniform in rapidity) to the nominal material model, data and detailed simulation agree well, in all bins of rapidity and for

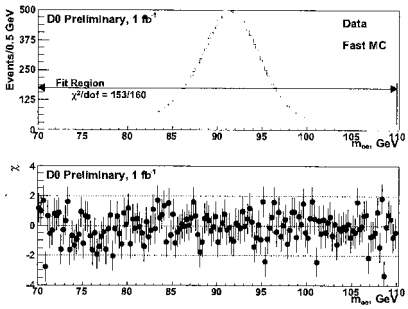

Figure 3: The Z mass distribution in DØ data and from the fast simulation (top) and the χ values for each bin (bottom). For a given bin, the χ value is defined as the difference between data and prediction, divided by the uncertainty on this difference. The error bars are set to unity. Here and in all other figures, the calculation of χ does not take into account systematic uncertainties in the parameter values in the fast simulation.

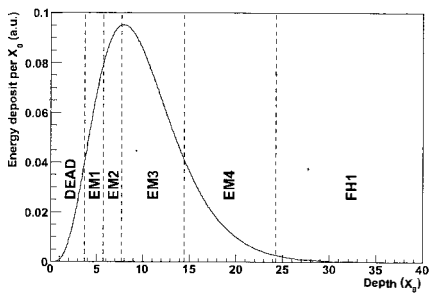

Figure 4: Illustration of partial sampling of showers in DØ Run II. The solid line represents the average profile of the longitudinal energy depositions from electron showers at $E = 45$ GeV. The positions of the four electromagnetic (EM) layers (EM1-EM4) and the first hadronic layer (FH1) of the DØ calorimeter, assuming normal incidence, are also indicated (dashed lines). The energy deposition is shown in arbitrary units.

all four readout sections. The energy-loss corrections and the model of sampling fluctuations used in this analysis are derived from the corrected first-principles simulation.

Once the electron energy scale and resolution are calibrated, we use the standard UA2 techniques [8] to transfer the electron energy calibration to the hadronic recoil. We build a parametric model of the hadronic recoil (this model describes the combined effect of fragmentation and detector response). As input to this model, we use various data control samples (*e.g.* random triggers collected during normal data taking to describe the effect of additional $p\bar{p}$ interactions in the same beam crossing, minimum bias triggers reweighted in scalar E_T ["event activity"] to the harder spectrum in Z events to model the effect of spectator quark interactions) as well as a first principles simulation for the hard component. We introduce free parameters in this model which are then adjusted to match the recoil E_T scale and resolution in the Z data. The observables used in the tuning are the mean and the width of the $\eta_{\rm lmb}$ distribution in bins of p_T^{ee}, where $\eta_{\rm lmb}$ is the sum of the recoil $\vec{u}_T$ and the $\vec{p}_T^{\,ee}$ vectors, projected on the $\hat{\eta}$ axis (Fig. 5).

Our three observables in DØ data are shown in Figs. 6 to 8. The systematic uncertainties are summarised in Tab. 1. The leading experimental systematics are mainly a reflection of the statistical limitation of the Z sample, and they are therefore expected to be significantly reduced once larger datasets are analysed. The uncertainties for the three observables are strongly correlated, albeit not fully. We combine the three results and obtain our new preliminary result: $m_W = 80.401 \pm 0.21(\text{stat}) \pm 0.038(\text{syst})$ GeV $= 80.401 \pm 0.043$ GeV. Figure 9 shows this result, previous results and the previous world average. The new DØ result is the most precise single measurement to date and it is in good agreement with the previous results.

8 Comparison to the first Run II measurement by CDF

The first Run II measurement of m_W by CDF has been published some time ago [1, 10]. We summarise the result and point out a few key differences compared to the DØ analysis. The CDF measurement is based on 200 pb^{-1} of early (*i.e.* low-luminosity) Run II data. It uses the same three observables as the DØ measurement, but in contrast to DØ, both $W \to e\nu$ and $W \to \mu\nu$ are used. The m_T distributions for the $\mu\nu$ and $e\nu$ channels are shown in Fig. 10, and the systematic uncertainties from the m_T observable are summarised in Tab.2. The final result (two channels

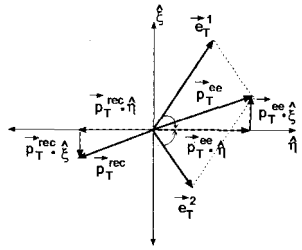

Figure 5: Definitions of the $\hat{\eta}$ and $\hat{\xi}$ axes for $Z \to ee$ events, as first defined by UA2 [8]. The $\hat{\eta}$ unit vector (not to be confused with the pseudorapidity) is coincident with the bisector of the two electron directions in the transverse plane, and $\hat{\xi}$ is perpendicular to $\hat{\eta}$. Here $\vec{p}_T^{\,\rm rec} = \vec{u}_T$, and $\vec{e}_T^{\,1}$, $\vec{e}_T^{\,2}$ denote the two electron momenta in the transverse plane.

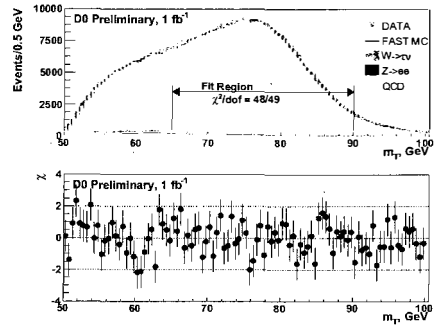

Figure 6: The m_T distribution for DØ data and the fast simulation with backgrounds added (top), and the χ value for each bin (bottom). The fit result is $m_W = 80.401 \pm 0.023$ (stat) GeV.

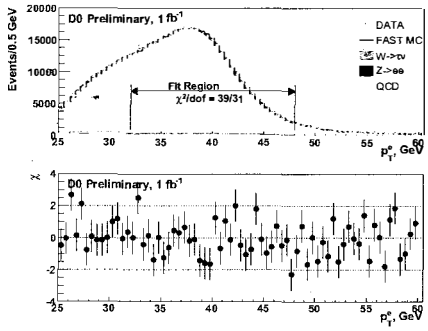

Figure 7: The p_T^e distribution for DØ data and the fast simulation with backgrounds added (top), and the χ value for each bin (bottom). The fit result is $m_W = 80.400 \pm 0.027$ (stat) GeV.

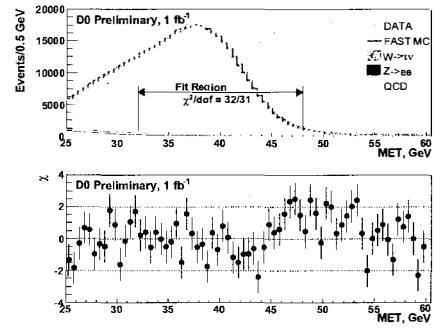

Figure 8: The p_T^{ν} distribution for DØ data and the fast simulation with backgrounds added (top), and the χ value for each bin (bottom). The fit result is $m_W = 80.402 \pm 0.023$ (stat) GeV.

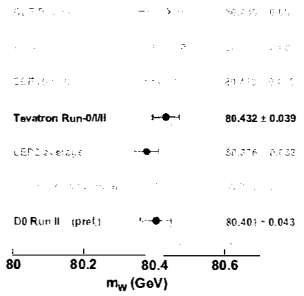

Figure 9: A comparison of the new DØ result, the world average (without the new result) and the measurements used in determining the world average [9].

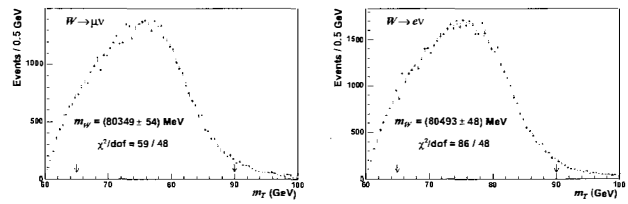

Figure 10: Transverse mass distributions from the CDF analysis: simulation (solid) and data (points) m_T distributions for W boson decays to $\mu\nu$ (left) and $e\nu$ (right). The simulation corresponds to the best-fit m_W, determined using events between the two arrows. The uncertainty is statistical only.

Source	m_T	p_T^e	$\not\!\!E_T$
Syst. (experimental)			
Electron Energy Scale	34	34	34
Electron Energy Resolution Model	2	2	3
Electron Energy Nonlinearity	4	6	7
W and Z Electron energy loss differences	4	4	4
Recoil Model	6	12	20
Electron Efficiencies	5	6	5
Backgrounds	2	5	4
Syst. (experimental) Total	35	37	41
Syst. (W production and decay model)			
PDF	9	11	14
QED	7	7	9
Boson p_T	2	5	2
Syst. (W model) Total	12	14	17
Syst. Total	37	40	44
Statistical	23	27	23
Total (Stat.+Syst.)	44	48	50

Table 1: Uncertainties in units of MeV in the DØ measurement of m_W, separately for the three observables. The big box summarises the systematic uncertainties. The two small boxes at the bottom show the statistical uncertainties and the total (stat.+syst.). The dominant systematic uncertainty comes from the electron energy scale, and this is determined by the statistical power of the Z event sample.

Source	$W \to \mu\nu$	$W \to e\nu$	Corr.
Tracker Momentum Scale	17	17	100%
Calorimeter Energy Scale	0	25	0%
Lepton Resolution	3	9	0%
Lepton Efficiency	1	3	0%
Lepton Tower Removal	5	8	100%
Recoil Scale	9	9	100%
Recoil Resolution	7	7	100%
Backgrounds	9	8	0%
PDF	11	11	100%
Boson p_T	3	3	100%
QED	12	11	100%
Statistical	54	48	0%
Total	60	62	-

Table 2: Uncertainties in units of MeV on the m_T fit for the $W \to \mu\nu$ and $W \to e\nu$ samples in the CDF measurement. The last column shows the correlation of the uncertainties between the two channels.

and three observables combined) is $40.413 \pm 0.034\,(\text{stat}) \pm 0.034\,(\text{syst}) = 40.413 \pm 0.048$ GeV.
The CDF analysis does not only include the muon channel, in fact central tracking is the key to this analysis, for both channels. This makes it very different from the DØ analysis. The central tracking system is aligned using cosmic events, and its absolute momentum scale is then set using $J/\psi \to \mu\mu$ and $\Upsilon \to \mu\mu$ data. The small energy loss corrections for muons are accounted for in the detector model. Fig. 11 shows the J/ψ control sample in one bin of $\langle 1/p_T^\mu \rangle$ ($1/p_T^\mu$ is proportional to track curvature, the "natural" variable for tracking studies). The tracking momentum scale as a function of $\langle 1/p_T^\mu \rangle$ is shown in Fig. 12. This result is combined with an assessment of the scale correction from the comparatively small, but higher-p_T^μ Υ sample. The final uncertainties in the momentum scale (*e.g.* 0.25×10^{-3} for the J/ψ) are largely dominated by systematic uncertainties (mainly the effects of QED and energy loss on the J/ψ and Υ lineshapes, as well as magnetic field nonuniformities). Using this momentum scale, the measured m_Z is consistent with the known m_Z from LEP, albeit within very large statistical uncertainties.
The tracking momentum scale is then transferred to the calorimeter-based energy scale for electrons using fits to the E/p peak from electrons in W and Z events, in bins of electron p_T (Figs. 13 and 14). The result is then combined with an energy scale estimate from the $Z \to ee$ mass peak; the latter has a weight of $\sim 30\%$ in the combination.
The use of mainly the huge J/ψ sample to set the tracking momentum scale explains why the CDF analysis achieves very competitive uncertainties using a small dataset. The disadvantages include the fact that the extrapolation of the lepton energy scale from the J/ψ to the W is much "farther" than the small extrapolation from the Z to the W. Furthermore, a scale calibration based on the Z sample alone explicitly exploits the similarities between the W and Z processes, *e.g.* in terms of FSR, energy flow into the electron window, etc. This can be seen, *e.g.*, in the QED uncertainties that are significantly smaller in the DØ analysis (Tabs. 1 and 2).

4 Direct measurement of the W boson charge asymmetry by CDF

As we have seen above, the PDF uncertainties are an important contribution to the m_W uncertainties due to the W production model. Other measurements of W production properties at the Tevatron can help reduce these uncertainties. One such measurement is the W charge asymmetry. Given that the dominant W production process at the Tevatron is $u\bar{d} \to W^+ + \text{c.c.}$

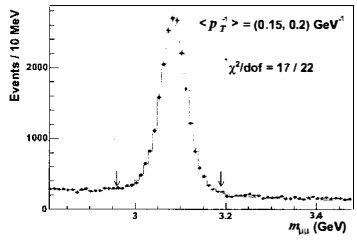

Figure 11: Fit to the CDF $J/\psi \rightarrow \mu\mu$ data in one bin of $\langle 1/p_T^{\mu} \rangle$ (averaged over the two muons from J/ψ) that is shown here as an example. The best fit corresponds to a fractional momentum scale correction of $(-1.54 \pm 0.09) \times 10^{-3}$. The arrows indicate the fit region and the errors are statistical only.

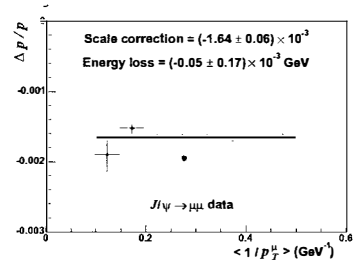

Figure 12: Fractional momentum scale correction for CDF data as a function of the mean inverse momentum of the muons from J/ψ decays. In a linear fit, the intercept corresponds to the scale correction relevant for W and Z boson decays, and the slope corresponds to the remaining unmodelled ionisation energy loss after tuning of the material model. The uncertainties are statistical only.

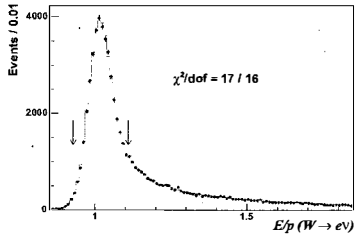

Figure 13: Energy scale calibration using the peak E/p region (denoted by arrows) in CDF $W \rightarrow e\nu$ data (points).

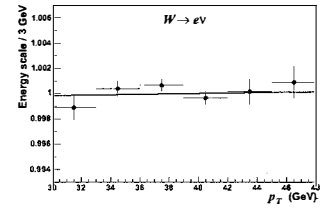

Figure 14: Energy scale as a function of measured electron calorimeter p_T^e for $W \rightarrow e\nu$ decays in CDF data. The fast simulation incorporates a per-particle non-linear response correction, tuned to the combination of this plot and its (low-statistics) equivalent for $Z \rightarrow ee$ data.

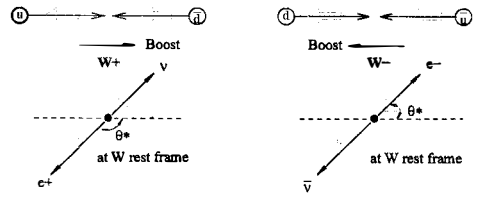

Figure 15: The momenta (arrows) and helicities (large outlines of arrows) in $p\bar{p} \rightarrow W^{\pm}$ production and $W^{\pm}$ leptonic decay at leading order.

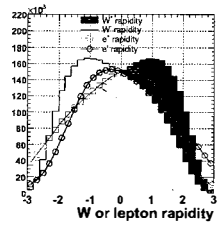

Figure 16: The boson and lepton rapidity distributions in $p\bar{p}$ collisions.

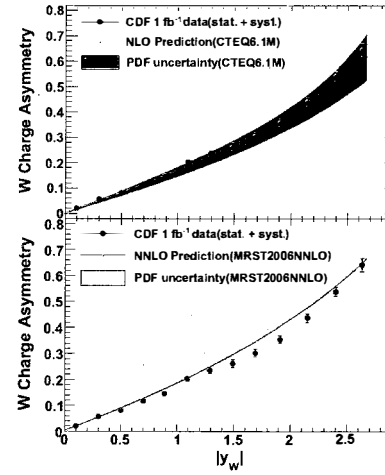

Figure 17: The measured W charge asymmetry from 1 fb^{-1} of CDF data, compared to predictions using two recent PDF sets and their uncertainties.

and that u and d quarks have different momentum distributions, W^+ and W^- are produced asymmetrically (Fig. 15). The resulting difference in the boson rapidity distributions is shown in Fig. 16. The charged leptons from W decay also reflect this asymmetry, but it is significantly reduced by the V-A nature of the weak interaction (Fig. 16). Previous measurements measured the lepton charge asymmetry. A new study [11] by CDF uses a new technique to measure the W charge asymmetry directly. To do so, one needs to reconstruct the boson rapidity, *i.e.* an estimate of the neutrino four-vector. The new measurement uses $W \to e\nu$ and the neutrino four-vector is obtained to within a two-fold ambiguity using the measured $\not\!\!E_T$ and the W mass constraint, $m(e\nu) = m_W$. Despite these complications, the novel technique works well, and systematic uncertainties on the asymmetry below 1.5% are achieved for boson rapidities below 2.0 . The measured asymmetry, as well as predictions based on current PDF sets and their uncertainties are shown in Fig. 17. From a comparison of the data and the predictions, we expect that this measurement will have an impact on future PDF sets and their uncertainties.

5 Conclusion and outlook

We have discussed the first Run II measurements of m_W from DØ and CDF. The DØ measurement has been shown for the first time at this conference, and it is already the single most precise measurement to date. Both measurements use only a small fraction of the datasets that the two collaborations have accumulated, and large improvements are expected from the use of larger datasets. CDF predict a total uncertainty of 25 MeV using 2.3 fb^{-1} and DØ predict even smaller uncertainties using the full 6 fb^{-1} that have been accumulated so far. A combined uncertainty at the level of 15 MeV at the end of Run II seems to be in reach. At this level, improvements in the theoretical description of W production and decay are needed. CDF and DØ contribute to this effort via measurements like the W charge asymmetry. At the same time, the theory community is maintaining a strong push that needs to be supported. If the central value remains the same, then the SM could be in serious difficulties at the end of Run II: for $\Delta m_W = 15$ MeV and $\Delta m_t = 1$ GeV, one would expect [12] m_H *o* 117 GeV at 95% CL, which would be inconsistent with lower limits from direct searches expected by that time.

Acknowledgments

It is a pleasure to thank my CDF and DØ colleagues for the exciting and fruitful collaboration, our Tevatron colleagues for the excellent luminosity, and the organisers for the nice conference.

References

1. CDF Collaboration, T. Aaltonen *et al.*, *Phys. Rev.* D **77**, 112001 (2008).
2. S. Heinemeyer, W. Hollik, D. Stockinger, A.M. Weber and G. Weiglein, `hep-ph/0604147`.
3. A.V. Kotwal and J. Stark, *Annu. Rev. Nucl. Part. Sci.* **58**, 147 (2008).
4. DØ Collaboration, `http://www-d0.fnal.gov/Run2Physics/WWW/results/prelim/EW/E27/` (2009).
5. C. Balazs and C.P. Yuan, *Phys. Rev.* D **56**, 5558 (1997).
6. H.L. Lai *et al.*, *Phys. Rev.* D **55**, 1280 (1997); J. Pumplin *et al.*, *JHEP* **0310**, 046 (2003).
7. E. Barbiero and Z. Was, *Comp. Phys. Commun.* **79**, 291 (1994).
8. UA2 Collaboration, J. Alitti *et al.*, *Phys. Lett.* B **276**, 354 (1992).
9. LEP Electroweak Working Group, CERN-PH-EP/2008-20, `arXiv:0811.4682` (2008); Tevatron Electroweak Working Group, FERMILAB-TM-2415 (2008).
10. CDF Collaboration, T. Aaltonen *et al.*, *Phys. Rev. Lett.* **99**, 151801 (2007).
11. CDF Collaboration, T. Aaltonen *et al.*, *Phys. Rev. Lett.* **102**, 181801 (2009).
12. P. Renton, contribution to the ICHEP 08 conference, `arXiv:0809.4566` (2008).